3
(Anti)kaon condensation in dense matter

3.1 Introduction

Nuclear matter is composed of mainly neutrons with small admixture of protons and electrons in β-equilibrium condition and fraction of protons are electrons are equal to keep the condition of charge neutrality. With the increase of neutron density the electron density and hence the Fermi momentum increases to keep the matter in β-equilibrium. With further increase of density when the electron Fermi energy reaches the vacuum mass of mesons (pion or kaon), condensate of negatively charged mesons is one of the several possible transitions which in turn help to maintain the charge neutrality. Even though the pion mass is significantly lower in comparison with kaons, s-wave πN scattering potential being repulsive the effective ground state mass of π-meson increases [Glendenning, 1985] opposing the possibility of π-meson appearing. Thus, in this thesis work, we have not included the pion contribution in dense matter systems. While, (anti)kaon condensation could exist by the processes $n \rightarrow p + K^-$ and $N \rightarrow N + \bar{K}^0$ with N representing the nucleons. The effective ground state mass of K-meson decreases due to its attractive interaction with nucleons opening the possibility of K-meson appearing.

Kaplan and Nelson [Nelson and Kaplan, 1987; Kaplan and Nelson, 1988] for the very first time demonstrated that (anti)kaon K^- may undergo Bose-Einstein condensation in dense matter formed in heavy-ion collisions. The K^--nucleon interaction was explained based on minimal coupling model in refs.-Glendenning and Schaffner-Bielich [1998, 1999] and we follow this approach in our studies. Furthermore, other evidences such as the K^- atomic data, kaon-nucleon scattering data [Brown et al., 1994; Lee et al., 1994, 1995] studied by several authors in chiral perturbation theory also encouraged the concept of K^- condensed phase presence in the interior of NS. The in-medium energy of (anti)kaon K^- mesons decreases in the dense matter due to the lowering of effective mass. Finally, the onset of s-wave K^- condensation occurs when the chemical potential of K^- (ω_{K^-}) equates the electron chemical potential (μ_e). The s-wave $\bar{K}^0$ appears when its chemical potential ($\omega_{\bar{K}^0}$) equates to zero. The threshold density of (anti)kaon appearance is very sensitive to the optical potential in nuclear symmetric matter. Studies Brown et al. [1994]; Lee et al. [1994]; Knorren et al. [1995]; Schaffner and Mishustin [1996] reveal that K^+ mesons develop a repulsive optical potential nature in nuclear matter. Thus, it may be concluded that kaon K^+ condensation is not favored inside the NS. Phase transitions from hadronic to kaonic phases in dense matter may be either a first or second order type depending on the (anti)kaon optical potential depths. The first order phase transition may result in a mixed phase region depending on the surface tension between the two phases. If the

surface tension is low, mixed phase is favoured while higher values of surface tension rejects mixed phase regime. Since the value of surface tension between the (anti)kaons and nucleons is not ascertained, we consider the same to be via low and study the nucleon-(anti)kaon mixed phase regime. Various observational features of NS evolution such as the spin down rates, cooling and glitches may be affected by the alterations of weak interaction rates and transport properties of matter interior to NS due to phase transitions Heiselberg and Hjorth-Jensen [2000]; Kubis and Kutschera [2003]. If the surface tension between the two phases is low, then the first order phase transition cannot be explained by merely the Maxwell's construction accounting for only one charge conservation because NSs have two conserved charges viz. baryon number conservation and global charge neutrality. The Gibbs conditions are employed to adequately explain the mixed phase regime of the NS interior Glendenning [1996]. However this is not true if the surface tension is large between the two phases which will then eradicate the possibility of mixed phase.

The onset of (anti)kaons in compact star matter is very sensitive to the K^- optical potentials and affects many properties of compact stars beyond the equation of state, such as superfluidity [Xu et al., 2018], neutrino emission via direct Urca processes [Ding et al., 2009; Xu et al., 2020] and bulk viscosity [Chatterjee and Bandyopadhyay, 2008]. This is a direct consequence of the changes in the single-particle spectrum of fermions, e.g., the Fermi momenta, effective masses, etc.

The formalism to introduce (anti)kaons in non-linear scalar as well as density-dependent RMF models and study the phase transition from hadronic to anti-kaon condensed matter is presented in next section (refer to sec.-3.2). This is followed by discussing the (anti)kaon coupling parameter estimations in sec.-3.3 and results in sec.-3.4. Finally the summary along with conclusions are outlined in sec.-3.5. This chapter is based on the work Thapa and Sinha [2020].

3.2 Formalism

The theoretical framework for the nuclear sector is already described in sec.-2.1. In this section, we introduce the RMF model to study the (anti)kaon condensed matter phase. The strong interactions between the (anti)kaons are mediated by the exchange of scalar σ, isoscalar-vector ω^μ and isovector-vector $\rho^{\mu\nu}$ meson fields. The Lagrangian for the (anti)kaons reads as

$$\mathcal{L}_K = D^*_\mu \bar{K} D^\mu K - m^{*^2}_K \bar{K} K \tag{3.1}$$

where $\bar{K} \equiv K^-, \bar{K}^0$, (anti)kaon effective mass, $m^*_K = m_K - g_{\sigma K}\sigma$ with $m_K = 495$ MeV denoting the bare (anti)kaon mass and the covariant derivative is given by

$$D_\mu = \partial_\mu + ig_{\omega K}\omega_\mu + ig_{\rho K}\boldsymbol{\tau}_K \cdot \boldsymbol{\rho}_\mu. \tag{3.2}$$

The scalar meson coupling to (anti)kaon is coupled similar to a minimal coupling scheme following ref.-Glendenning and Schaffner-Bielich [1999]. The equation of motion for (anti)kaons can be written as

$$[D_\mu D^\mu + m^*_K]K = 0. \tag{3.3}$$

Considering infinite matter, the plane wave solution of eq.-(3.3) is given by $K \sim e^{-i\omega_K t}\kappa$ which reduces eq.-(3.3) to the form

$$[-\omega_K^2 + m_K^2 + \Pi_K(\omega_K, \boldsymbol{k})]\kappa = 0 \tag{3.4}$$

where $\boldsymbol{k}$ denotes the 3-momentum of (anti)kaons and the self energy of K^- denoted by $\Pi_K(\omega_0, \boldsymbol{k})$ is given by

$$\Pi_K = -2\omega_K \left(g_{\omega K}\omega_0 + \frac{1}{2} g_{\rho K}\rho_{03} \right) - \left(g_{\omega K}\omega_0 + \frac{1}{2} g_{\rho K}\rho_{03} \right)^2 - 2m_K g_{\sigma K}\sigma + (g_{\sigma K}\sigma)^2 \tag{3.5}$$

In the MFA, the in-medium energies of $\bar{K} \equiv (K^-, \bar{K}^0)$ for s-wave condensation ($\boldsymbol{k} = 0$) are provided by substituting eq.-(3.5) in eq.-(3.4)

$$\omega_{K^-,\bar{K}^0} = m_K^* - g_{\omega K}\omega_0 \mp \frac{1}{2} g_{\rho K}\rho_{03} \tag{3.6}$$

with the isospin projections for $K^-, \bar{K}^0$ being $-1/2, +1/2$ respectively. Within MFA, the meson fields acquire the ground state expectation values

$$\begin{aligned}
\sigma &= -\frac{1}{m_\sigma^2}\frac{\partial \mathrm{U}}{\partial \sigma} + \sum_N \frac{1}{m_\sigma^2} g_{\sigma N} n_N^s + \sum_{\bar{K}} \frac{1}{m_\sigma^2} g_{\sigma K} n_{\bar{K}}, \\
\omega_0 &= \sum_N \frac{1}{m_\omega^2} g_{\omega N} n_N - \sum_{\bar{K}} \frac{1}{m_\omega^2} g_{\omega K} n_{\bar{K}}, \\
\rho_{03} &= \sum_N \frac{1}{m_\rho^2} g_{\rho N} \boldsymbol{\tau}_{N3} n_N + \sum_{\bar{K}} \frac{1}{m_\rho^2} g_{\rho K} \boldsymbol{\tau}_{\bar{K}3} n_{\bar{K}}
\end{aligned} \tag{3.7}$$

where, the first term in right hand side of eq.-(3.7) (σ-meson field) is required only in the case of non-linear scalar model while it is absent in case of density-dependent model. The number density in case of the s-wave (anti)kaon condensates evaluated from the conserved current associated with (anti)kaons is given by

$$\begin{aligned}
n_{K^-,\bar{K}^0} &= 2\left(\omega_{\bar{K}} + g_{\omega K}\omega_0 \pm \frac{1}{2} g_{\rho K}\rho_{03} \right) \\
&= 2m_K^* \bar{K} K.
\end{aligned} \tag{3.8}$$

For the (anti)kaon condensates, the energy density contribution to the total one is given by

$$\varepsilon_{\bar{K}} = m_K^*(n_{K^-} + n_{\bar{K}^0}). \tag{3.9}$$

(Anti)kaons being Bose condensates, there is no direct contribution to the total matter pressure from their ends. Due to the inclusion of (anti)kaons, the charge neutrality condition is modified as, $n_p - n_{K^-} - n_e - n_\mu = 0$.

Studies Prakash et al. [1997]; Glendenning [1996] show that strangeness changing processes such as, $N \rightleftharpoons N + \bar{K}$ and $e^- \rightleftharpoons K^-$ may come into picture inside the neutron star core. Hence, (anti)kaons may appear by these reactions, when the threshold conditions are satisfied as

$$\mu_n - \mu_p = \omega_{K^-} = \mu_e, \quad \omega_{\bar{K}^0} = 0. \tag{3.10}$$

3.2.1 Mixed phase regime

The EoS of matter interior to compact objects is characterized by matter phase transitions. In the case of (anti)kaon condensation, the matter phase transition may occur through either first order (this form of phase transition is triggered by the implicit behaviour as decrease in neutron chemical potential with rising matter density) or second order depending upon the (anti)kaon optical potential in nuclear symmetric matter [Glendenning, 1996]. Glendenning [1992] treated the phase equilibrium in the case of multi-component or, multiple chemical potentials corresponding to the conserved quantities via Gibbs conditions. In this treatment of first order phase transition, the global charge neutrality condition is considered in lieu of local one. As a result, the matter pressure increases monotonously in the interior to dense matter.

In case of the phase transition being first order, a mixed phase could come into picture: the two phases of pure hadronic matter without condensate and with condensate could coexist. Then for this case, the Gibbs conditions alongside global baryon number conservation and charge neutrality can be enforced to determine the mixed phase state [Glendenning, 1992; Glendenning and Schaffner-Bielich, 1998]. The Gibbs conditions for this state are given by,

$$\begin{aligned} P^h &= P^{\bar{K}} \quad \text{(Pressure equilibrium)}, \\ \mu_N^h &= \mu_N^{\bar{K}} \quad \text{(Chemical equilibrium)}, \end{aligned} \tag{3.11}$$

where h and $\bar{K}$ superscripts represent the respective quantities in hadronic and (anti)kaon condensed phase respectively. Since we are considering cold dense matter EoS, so the thermal equilibrium condition may be not brought into picture in this particular scenario. The two additional global constraints (viz. global baryon number conservation and charge neutrality) are modified in both the phases as

$$\begin{aligned} n_N &= (1-\chi) n_N^h + \chi n_N^{\bar{K}}, \\ (1-\chi) Q^h &+ \chi Q^{\bar{K}} = 0 \end{aligned} \tag{3.12}$$

respectively. Here, χ is the fraction of (anti)kaon (K^-) condensed phase in the mixed phase regime. The beginning and end of mixed phase region are signalled by $\chi = 0, 1$ respectively. Region with $\chi < 0$ is the pure hadronic phase and $\chi > 1$ is the (anti)kaon condensed phase. In the mixed phase, the total energy density also changes the form to

$$\varepsilon = (1-\chi)\varepsilon^h + \chi \varepsilon^{\bar{K}} \tag{3.13}$$

where, ε^h, $\varepsilon^{\bar{K}}$ denotes the total energy density in hadronic and (anti)kaon phases respectively.

3.3 Coupling parameters

In this work to study the role of (anti)kaon condensation in NS matter, we adopt GMT [Pal et al., 2000a] and NL3 [Lalazissis et al., 1997] coupling parametrizations in non-linear scalar scheme while in case of density-dependent model we consider DD2 [Typel et al., 2010], DD-ME2 [Lalazissis et al., 2005] and PKDD [Long et al., 2004] coupling parameter sets to describe the meson-nucleon interactions. The coupling values of the parameter sets considered in this work are provided in tables-2.1 and 2.3.

Table 3.1: Parameter values of the scalar σ meson-(anti)kaon couplings in different parametrizations at n_0 considered in this study.

$U_{\bar{K}}(n_0)$	$g_{\sigma K}$				
(MeV)	GMT	NL3	DD-ME2	DD2	PKDD
-120	0.8217	0.4707	0.4311	0.3155	0.4309
-140	1.4006	1.0088	0.9553	0.8359	0.9639
-160	1.9796	1.5469	1.4796	1.3562	1.4970

3.3.1 (Anti)kaon coupling constants

To explore the effect of (anti)kaons on dense matter, parametrizing the meson-(anti)kaon as well as (anti)kaon-nucleon interactions are essential. In order to do so, we need to specify the meson-(anti)kaon coupling values. The meson-(anti)kaon couplings are not considered to be density-dependent following ref.-Char and Banik [2014] in density-dependent RMF model. The vector coupling parameters (*i.e.* the coupling with ω and ρ mesons) in the (anti)kaon sector are evaluated from the iso-spin counting rule and quark model [Glendenning and Schaffner-Bielich, 1999; Banik and Bandyopadhyay, 2001] as

$$g_{\omega K} = \frac{1}{3} g_{\omega N}, \quad g_{\rho K} = g_{\rho N}. \tag{3.14}$$

And for the scalar coupling parameters (*i.e.* with σ meson), they are calculated at nuclear saturation density from the real part of K^- optical potential depth of a single (anti)kaon in infinite matter as

$$U_{\bar{K}}(n_0) = -g_{\sigma K}\sigma(n_0) - g_{\omega K}\omega_0(n_0) + \Sigma_N^r(n_0) \tag{3.15}$$

where, $\Sigma_N^r(n_0)$ is the contribution from the nucleons alone and is not considered in case of non-linear scalar RMF model.

Studies Li et al. [1997]; Pal et al. [2000b] show that the kaons experience a repulsive interaction in nuclear matter whereas (anti)kaons experience an attractive potential. Several model calculations Koch [1994]; Waas and Weise [1997]; Lutz [1998]; Ramos and Oset [2000]; Schaffner-Bielich et al. [2000] provide a very broad range of optical potential values as $-120 \leq U_{\bar{K}} \leq -40$ MeV. Another calculation from a hybrid model based on a theoretically motivated RMF approach and a phenomenological density dependent potential satisfying the low density theorem in the nuclear surface region [Friedman et al., 1999] suggests the value of K^- optical potential to be in the range 180 ± 20 MeV at nuclear saturation density. In this work, we have considered a K^- potential range of $-160 \leq U_{\bar{K}} \leq -120$ MeV and the scalar meson-(anti)kaon couplings evaluated for the above potential depth range are listed in table-3.1.

3.4 Results and discussions

The coupling parameter sets considered in this work satisfy the nuclear saturation properties obtained from various model calculations based on certain experimental data. In this section, we present the results of the possibility of (anti)kaon in dense nuclear matter evaluated with the framework of RMF theory and considering different (anti)kaon optical potentials as $U_{\bar{K}} = -120, -140, -160$ MeV.

3.4.1 Non-Linear scalar RMF model

In the case of GMT parametrization, the transition from hadronic to kaonic phase is observed to be of second order for $U_{\bar{K}} = -120, -140$ MeV but of first order for $U_{\bar{K}} = -160$ MeV. While in case of NL3 parameterization, the phase transition is of second order for the whole range of K^- potential adopted here.

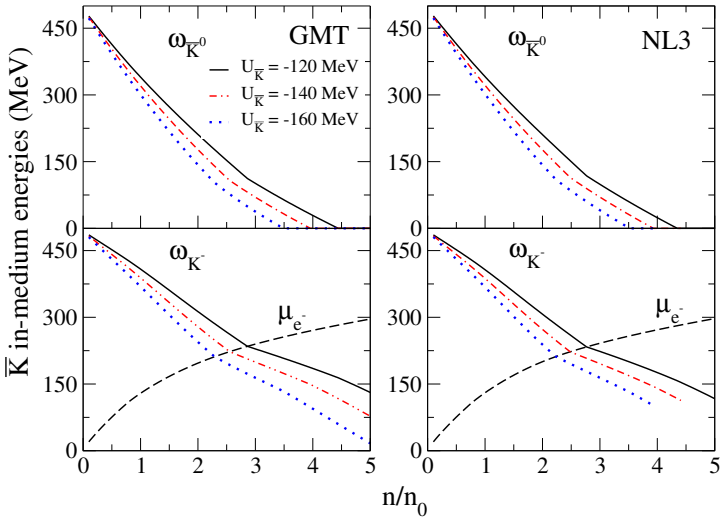

Figure 3.1: The effective energy of (anti)kaons as a function of baryon number density, left panels: GMT, right panels: NL3 parametrization. Upper panels: in-medium energies of $\bar{K}^0$, lower panels: in-medium energies of K^- with several $U_{\bar{K}}$. The dashed lines represent the respective electron chemical potentials for each model case. The solid curve exhibits the $U_{\bar{K}}$ strengths of -120 MeV, dash-dotted lines exhibits -140 MeV case and dotted lines exhibits the -160 MeV case.

The (anti)kaon energies as a function of baryon number density with $U_{\bar{K}} = -120, -140, -160$ MeV for the two parameter sets (GMT, NL3) are shown in fig.-3.1. The in-medium energies for both the (anti)kaons decrease with density. The dashed curve representing μ_e crossing over the $\omega_{\bar{K}}$ curves marks the end of pure hadronic phase and initiation of (anti)kaonic phase. K^- condensations initiates once the value of ω_{K^-} reaches that of the electron chemical potential and $\bar{K}^0$ condensation starts when the value of $\omega_{\bar{K}^0}$ equates to zero. It is observed that the threshold condition, $\omega_{K^-} = \mu_e$ is achieved way earlier than $\omega_{\bar{K}^0} = 0$ one, leading to earlier appearance of K^-.

Fig.-3.2 shows the matter pressure as a function of energy density for both the GMT and NL3 models. The appearance of (anti)kaons to a great extent softens the EoS. The two kinks in the EoSs marks the onset of K^- and $\bar{K}^0$ respectively. The two kinks are observed to be in higher densities for the NL3 model in comparison to the GMT case referring the delay of (anti)kaons into the matter for the former case. The appearance of (anti)kaon condensation is through first order transition only for K^- with $U_{\bar{K}} = -160$ MeV in GMT parametrization. In other cases it is second order phase transition.

The variation of particle fractions with total baryonic number density is shown in the fig.-3.3 for $U_{\bar{K}}(n_0) = -160$ MeV for both the parametrization sets. Inspite of large rest mass of (anti)kaons compared to the lepton species and being bosons, the former condense in the lowest

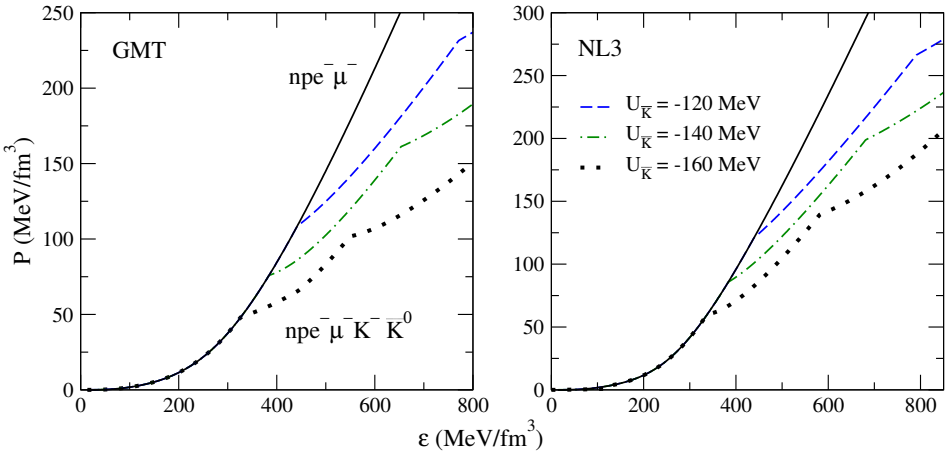

Figure 3.2: The variation of matter pressure with energy density. Left panel: GMT parameterization, right panel: NL3 parameterization cases with several (anti)kaon potential depths ($U_{\bar{K}}$). The solid lines represent the composition of only nucleons (n, p) and leptons (e^-, μ^-). The other curves represent the composition with (anti)kaons in addition to nucleons and leptons. The dashed curve depicts $U_{\bar{K}} = -120$ MeV, dash-dotted curve with $U_{\bar{K}} = -140$ MeV and dotted curve with $U_{\bar{K}} = -160$ MeV.

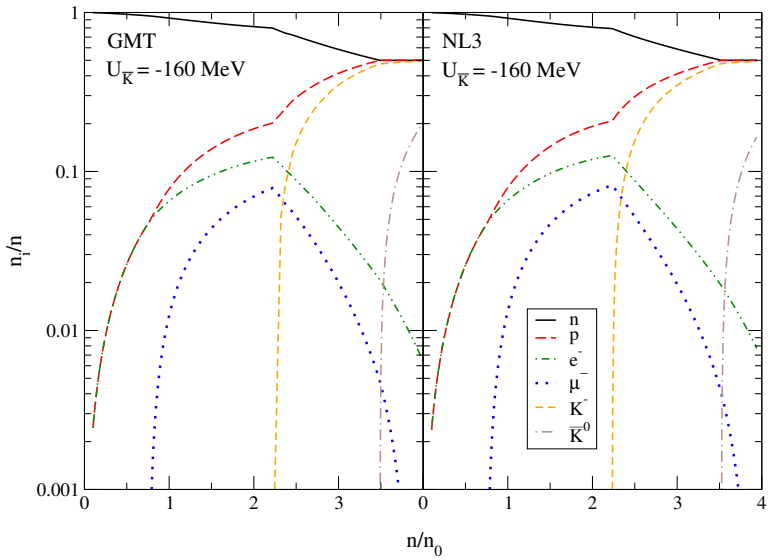

Figure 3.3: Population densities n_i (in units of n) of various species as a function of baryon number density. Left panel: GMT, right panel: NL3 model and K^- potential depth of -160 MeV. Solid lines denote neutron (n), long-dashed lines proton (p), dash-dotted curves electron (e^-), dotted lines muon (μ^-), short-dashed lines K^- and dash-double dotted lines denote $\bar{K}^0$ population.

energy state and so are preferred to maintain the global charge neutrality condition. This results in decrease in electron and muon populations as can be clearly visualized in fig.-3.3. Further, with appearance of $\bar{K}^0$ at $\sim 3.49\ n_0$ and ceasing of electron population around $4 - 4.5\ n_0$ the proton and K^- populations become equal following the charge neutrality condition. The

condensation of $\bar{K}^0$ is found to be through the second order phase transition. However, for NL3 coupling model the phase transition occurs via second order for both the (anti)kaons ($K^-, \bar{K}^0$) implying the absence of mixed phase regime. Even though we are fixing the $U_{\bar{K}}$ identical to GMT model cases, the (anti)kaons appear at a slightly higher densities compared to the former case. The threshold densities for the onset of $K^-, \bar{K}^0$ in the dense nuclear matter for different (anti)kaon optical potentials are provided in table-3.2. It can be observed that the threshold densities shift towards lower densities with the increase in strength of $U_{\bar{K}}$ at n_0.

Table 3.2: Threshold densities, n_{cr} for (anti)kaon condensation in dense nuclear matter for different values of K^- optical potential depths $U_{\bar{K}}$ at n_0.

	GMT		NL3	
$U_{\bar{K}}$ (MeV)	$n_{cr}(K^-)$ (n_0)	$n_{cr}(\bar{K}^0)$ (n_0)	$n_{cr}(K^-)$ (n_0)	$n_{cr}(\bar{K}^0)$ (n_0)
-120	2.87	4.45	2.77	4.35
-140	2.56	3.96	2.49	3.94
-160	2.22	3.49	2.24	3.53

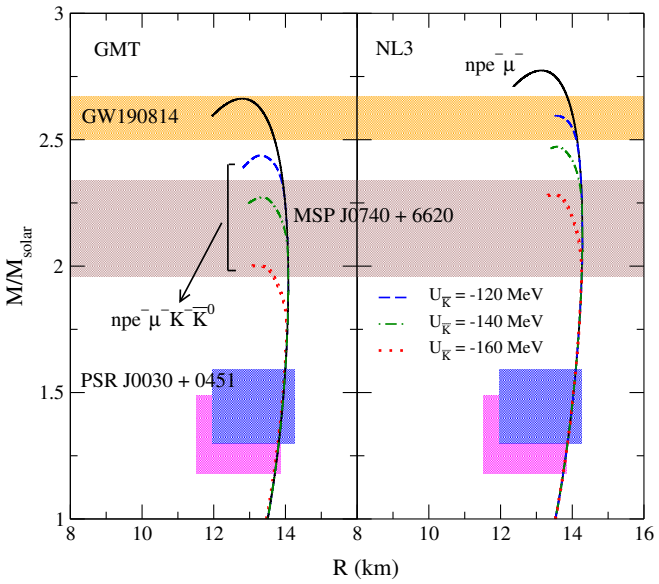

Figure 3.4: The mass-radius relations corresponding to the EoSs shown in fig.-3.2. Left panel: GMT, right panel: NL3 parameterization. The solid curve corresponds to the pure nucleonic star, while the dashed, dash-dotted, dotted curves correspond to stars with (anti)kaon condensation and optical potentials, $U_{\bar{K}} = -120, -140, -160$ MeV respectively. The mass constraints from the various astrophysical observations are represented by the shaded regions corresponding to the GW190814 observation [Abbott et al., 2020b], MSP J0740+6620 [Cromartie et al., 2020]. The mass-radius limits obtained for PSR J0030+0451 from the NICER experiment [Miller et al., 2019; Riley et al., 2019] are represented by the squared shaded regions.

Fig.-3.4 shows the results of the mass-radius (M-R) relationship for static spherical stars from solution of the Tolman-Oppenheimer-Volkoff (TOV) equations corresponding to the EoSs discussed here and shown in fig.-3.2. For the crust, we have considered the EoS of Baym, Pethick and Sutherland (BPS) [Baym et al., 1971b] and Baym, Bethe, Pethick (BBP) [Baym et al., 1971a]. Table-3.3 provides the set of maximum mass values, corresponding radius and

central density for the nucleons and (anti)kaon EOSs with various values of $U_{\bar{K}}$. Inclusion of (anti)kaons leads to reduction of maximum mass of the compact stars. In this particular work, the possibility of a third family of compact objects is not studied due to the reason that for a third family to come into picture the (anti)kaon potential needs to be high enough resulting in softer EoSs evaluating lower maximum mass NS configurations.

Table 3.3: Parameter values of the maximum mass stars from fig.-3.4. Here, maximum mass, M_{max}, radius and corresponding central density n_c of nucleon compact stars for different values of K^- optical potential depths $U_{\bar{K}}$ at n_0 in GMT and NL3 parametrization models.

	GMT			NL3		
$U_{\bar{K}}$ (MeV)	M_{max} ($M_\odot$)	R (km)	n_c (n_0)	M_{max} ($M_\odot$)	R (km)	n_c (n_0)
0	2.66	12.80	4.91	2.77	13.14	4.52
−120	2.44	13.31	4.76	2.59	13.56	4.37
−140	2.27	13.36	4.75	2.47	13.59	4.47
−160	2.00	13.22	4.78	2.28	13.48	4.53

First order phase transition

In our study, we observe that for GMT parametrization the mixed phase initiates with the onset of K^- at $\sim 2.22\ n_0$. The global conservation rule of baryon number and charge neutrality (eq.-(3.12)), pressure and chemical potential equilibrium conditions between two phases (eq.-(3.11)) determine the mixed phase region. Fig.-3.5 shows the extent of mixed phase region inside a 2 $M_\odot$ neutron star modelled with GMT parametrization. It is evident that the mixed phase regime starts ($\chi \sim 0$) from around matter density of $\sim 2.22\ n_0$ which corresponds to star radius 7.34 km, and terminates ($\chi \sim 1$) at around matter density of $2.9\ n_0$ or corresponding stellar radius of, ~ 6.13 km.

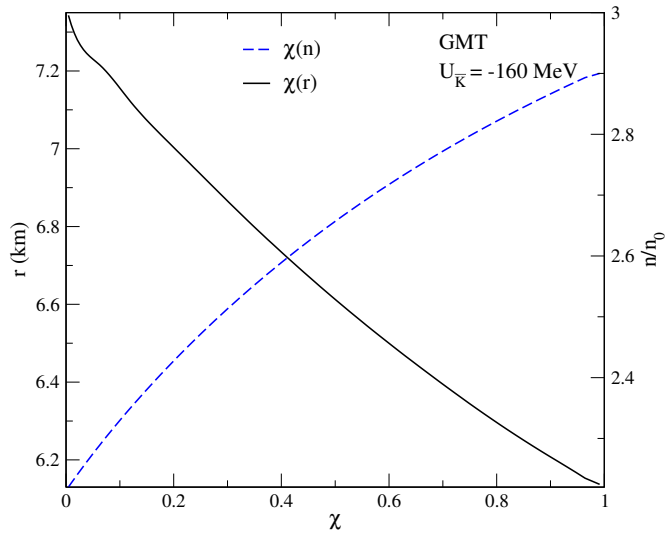

Figure 3.5: Baryon number density (n), radial distance (r) inside a 2 $M_\odot$ compact star as a function of volume fraction of the (anti)kaon condensate (χ) for the GMT model case with $U_{\bar{K}} = -160$ MeV. The solid curve denotes $\chi(r)$, while dashed curve represents $\chi(n)$.

The interactions between (anti)kaons and nucleons alters the nucleon effective mass in the mixed phase regime where both the hadronic and (anti)kaonic phase co-exist. This effect in shown in fig.-3.6. With a difference of ~ 100 MeV, the effective nucleon masses are observed to increase in (anti)kaonic phase while it decreases in the pure hadronic phase as we move interior towards the (anti)kaonic condensed phase regime.

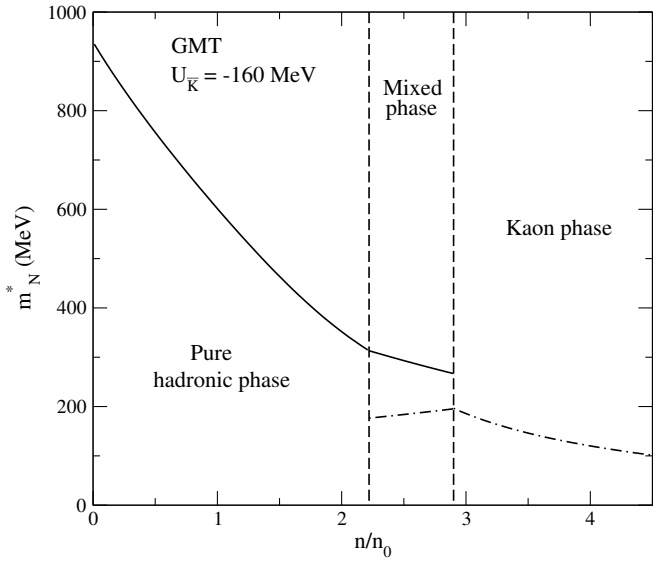

Figure 3.6: Effective nucleon mass, m^*_N as a function of baryon number density for the GMT model case with $U_{\bar{K}} = -160$ MeV. The solid curve denotes $m^*_N(n_B)$ in hadronic phase, while dash-dotted curve represents $m^*_N(n_B)$ in (anti)kaonic phase. Region with $n < 2.2\ n_0$ is the pure hadronic phase, between $2.2 \leq n \leq 2.9\ n_0$ is the mixed phase and $n > 2.9\ n_0$ is the (anti)kaonic phase.

The charge densities of each normal and kaon condensed phase in the mixed phase region for the GMT model with $U_{\bar{K}} = -160$ MeV as a function of the kaon volume fraction are shown in fig.-3.7. The central solid black line represents the global charge neutrality condition as provided in eq.-(3.12).

The difference in the energy densities of the hadronic and (anti)kaonic phases for GMT parameterization with $U_{\bar{K}} = -160$ MeV is shown in fig.-3.8. The total energy density in the mixed phase region is evaluated from eq.-(3.13) and grows monotonically with density.

3.4.2 Density-dependent RMF model

In case of density-dependent RMF model, the phase transition from hadronic to (anti)kaonic phase for all parametrizations and all (anti)kaon optical potential depths considered in our work is through the second-order phase transition.

Table-3.4 provides the threshold densities of (anti)kaon condensation in different potential depths of (anti)kaons. It can be observed from table-3.4 that the appearance of K^--mesons takes place earlier in case of DD-ME2 model irrespective of the optical potential. On the other hand, the appearance of $\bar{K}^0$ takes place early in PKDD model among others. With the increasing potential depth of (anti)kaons in symmetric nuclear matter, the onset of (anti)kaons happens earlier.

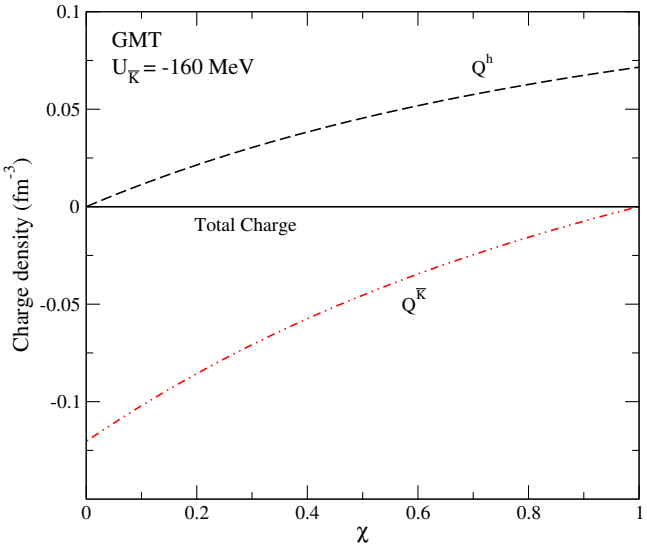

Figure 3.7: Charge densities in the pure hadronic phase and (anti)kaon condensed phase as a function of volume fraction of the latter for the GMT model case with $U_{\bar{K}} = -160$ MeV. $Q^h, Q^{\bar{K}}$ denote the charge in hadronic and kaonic phases respectively.

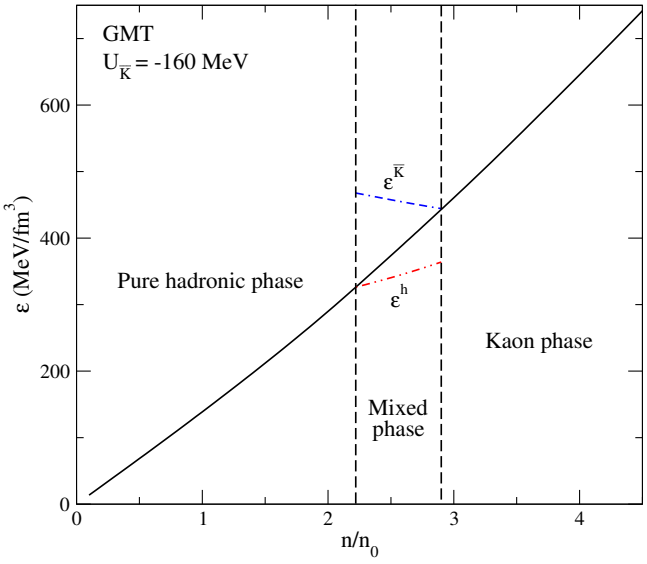

Figure 3.8: Energy density as a function of baryon number density for the GMT model with $U_{\bar{K}} = -160$ MeV for the three phases. The solid curve denotes the total energy density variation, while dash-dotted curves represent ε^h and dash-double dotted curve represent $\varepsilon^{\bar{K}}$. The three region demarcations are similar as fig.-3.6.

The matter pressure as a function of energy density for different density-dependent coupling models is shown in fig.-3.9. It is observed that the stiffest EoS results are for the DD-ME2 parametrization. Incorporation of $\bar{K}$ softens the EoS and more pronounced effects are seen with deeper K^- optical potential depths. The two kinks in the EoS marks the onsets of K^- and $\bar{K}^0$ respectively. While the first kink appears to be $\sim$ 400 MeV/fm^3 for all the three parametrizations, the onset of $\bar{K}^0$ denoted by the second kink is delayed the most in

Table 3.4: Threshold densities, n_{cr} for antikaon condensation in dense nuclear matter for different values of K^- optical potential depths $U_{\bar{K}}$ at n_0 with density-dependent DD-ME2, DD2, PKDD parametrizations.

	DD-ME2		DD2		PKDD	
$U_{\bar{K}}$ (MeV)	$n_{cr}^{K^-}(n_0)$	$n_{cr}^{\bar{K}^0}(n_0)$	$n_{cr}^{K^-}(n_0)$	$n_{cr}^{\bar{K}^0}(n_0)$	$n_{cr}^{K^-}(n_0)$	$n_{cr}^{\bar{K}^0}(n_0)$
-120	3.00	4.89	3.08	5.11	3.16	4.75
-140	2.72	4.42	2.79	4.62	2.82	4.29
-160	2.47	3.96	2.53	4.14	2.53	3.84

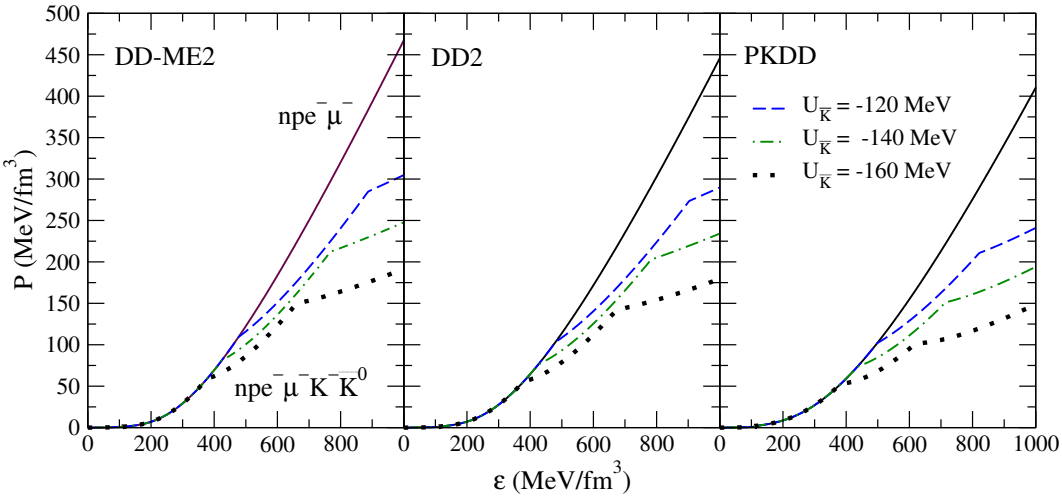

Figure 3.9: The equation of states, Left panel: DD-ME2, center panel: DD2, right panel: PKDD parametrization case with several (anti)kaon potential depths ($U_{\bar{K}}$). The solid lines represent the composition of only nucleons (n, p) and leptons (e^-, μ^-). The dashed curves depict $U_{\bar{K}} = -120$ MeV, dash-dotted curves with $U_{\bar{K}} = -140$ MeV and dotted curves with $U_{\bar{K}} = -160$ MeV represent the composition with (anti)kaons.

DD2 parametrization case.

Fig.-3.10 presents the results of mass-radius (M-R) relationship for static spherically symmetric stars by solving the TOV equations corresponding to the EoSs in fig.-3.9. The crust EoS is the same as considered in the NL CDF model. Table-3.5 provides the set of maximum mass, and corresponding radius and central density with different values of $U_{\bar{K}}$. For the stars with only nucleons and leptons, the maximum masses are 2.48, 2.42, 2.33 $M_\odot$ with DD-ME2, DD2 and PKDD parametrization respectively. The maximum mass of the compact stars decreases substantially with the inclusion of (anti)kaons. It is observed that configurations with DD-ME2 satisfy the observed maximum mas neutron star constraint of ~ 2 $M_\odot$ uptil $U_{\bar{K}} = -160$ MeV. For the other two model cases, DD2 satisfy the constraint uptil $U_{\bar{K}} = -140$ MeV, while PKDD providing a further softer EoS satisfy the constraint only upto $U_{\bar{K}} = -120$ MeV.

Fig.-3.11 represents the (anti)kaon energies as a function of baryon number density with $U_{\bar{K}} = -120$ MeV for the density-dependent coupling models. The onset of K^- and $\bar{K}^0$

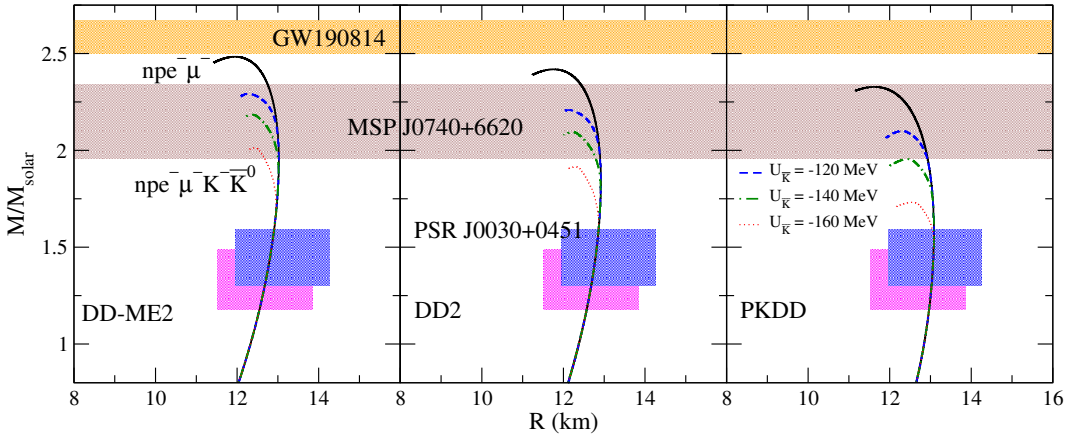

Figure 3.10: The TOV solutions corresponding to the EoSs in fig.-3.9. Left panel: DD-ME2, center panel: DD2, right panel: PKDD parametrization. The mass-radius constraints are similar as in fig.-3.4. The solid curve denotes the case with only nucleons and leptons, while the dashed curves correspond to $U_{\bar{K}} = -120$ MeV, dash-dotted curves represents $U_{\bar{K}} = -140$ MeV and dotted curves denote $U_{\bar{K}} = -160$ MeV case.

Table 3.5: Maximum mass, M_{max} (in units of $M_\odot$), radius (in km), corresponding central density (in units of n_0) of nucleon compact stars for different values of K^- optical potential depths $U_{\bar{K}}$ (in units of MeV) at n_0 in DD-ME2, DD2, PKDD parametrization models.

Model ↓	Parameters ↓	Config. → $U_{\bar{K}}$ (MeV) →	$npe\mu$	$npe\mu\bar{K}$		
			0	−120	−140	−160
DD-ME2	$M_{max}(M_\odot)$		2.48	2.29	2.18	2.01
	R (km)		11.96	12.28	12.37	12.43
	n_c (n_0)		5.36	5.37	5.33	5.22
DD2	$M_{max}(M_\odot)$		2.42	2.21	2.09	1.92
	R (km)		11.77	12.14	12.23	12.29
	n_c (n_0)		5.69	5.68	5.62	5.47
PKDD	$M_{max}(M_\odot)$		2.33	2.10	1.95	1.73
	R (km)		11.63	12.31	12.44	12.56
	n_c (n_0)		5.94	5.54	5.36	5.05

occurs with ω_{K^-} crossing over μ_{e^-} and $\omega_{\bar{K}^0}$ being equal to zero respectively. Similar behavior is observed in case of DD-ME2 and DD2 parametrization models, while for PKDD model, the K^- in-medium energy is higher compared to the other two cases and $\bar{K}^0$ in-medium energy is observed to be lower.

The population densities of different species, n_i (in units of n_0) in the neutron star interior as a function of baryon number density for the density-dependent models are provided in fig.3.12. (Anti)kaons, being bosons are not constrained by Pauli blocking, resulting in lepton fraction suppression at high density regions. The population behavior in two cases of DD-ME2 and DD2 are observed to be similar with slight difference in the threshold density of $\bar{K}$-meson appearance. The proton population (subsequently electron and muon) is higher at lower densities for PKDD model case compared to DD-ME2, DD2 models due to higher symmetry

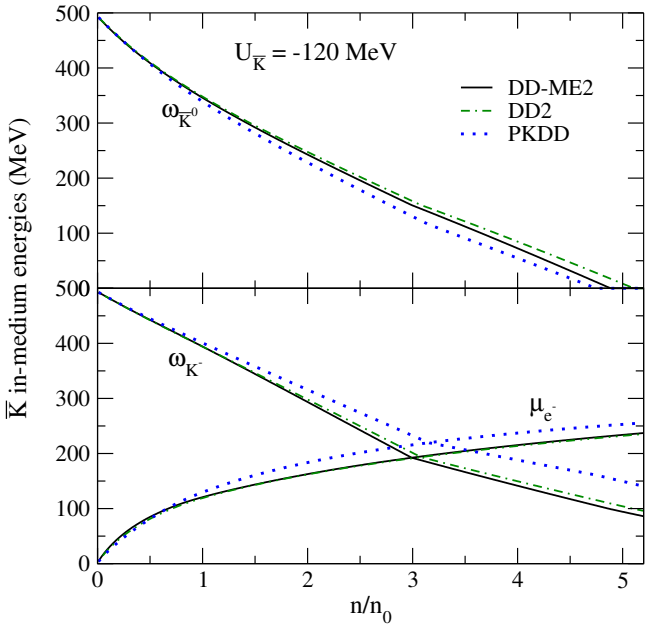

Figure 3.11: The effective energy of (anti)kaons as a function of baryon number density with $U_{\bar{K}} = -120$ MeV. Upper panel: for $\bar{K}^0$ and lower panel: for K^- with solid lines denoting DD-ME2, dash-dotted curves representing DD2 and dotted lines representing PKDD parametrization.

energy. For PKDD model, in addition to the early onset of $\bar{K}^0$ particles, the eradication of lepton species is quite delayed compared to the former parametrizations due to the abundance of more protons. This results in further softening of EoS.

3.5 Summary

In this chapter, we investigated the appearance of the (anti)kaon condensation in β-equilibrated charge neutral nucleonic matter within the framework of mean field theory with density-independent (non-linear scalar RMF model) as well as dependent (density-dependent RMF model) coupling constants.

Stars with mass near and above 2 $M_\odot$ must contain central density above 4 n_0. At such high density the phase transition to boson condensate within the nuclear matter is highly probable. However, the appearance of (anti)kaon condensation softens the EoS lowering the maximum mass of the NS family. We discuss here certain parametrizations of EoS within RMF model which are stiff enough to provide maximum mass above 2 $M_\odot$ with appearance of (anti)kaon condensation at the inner core of the star. We obtain the result that with non-linear model, GMT and NL3 parametrizations provide the required stiff EoS to have maximum mass 2 $M_\odot$ with all the (anti)kaon optical potential depth $U_{\bar{K}} = -120, -140, -160$ MeV. The (anti)kaon condensed star with $U_{\bar{K}} = -120$ MeV and NL3 coupling model satisfies the gravitational wave observation mass constraint from GW190814 even though it is uncertain as the star has not been identified as NS unambiguously [Abbott et al., 2020b; Sedrakian et al., 2020; Jie Li et al., 2020]. For density-dependent RMF model, the DD-ME2 parametrization

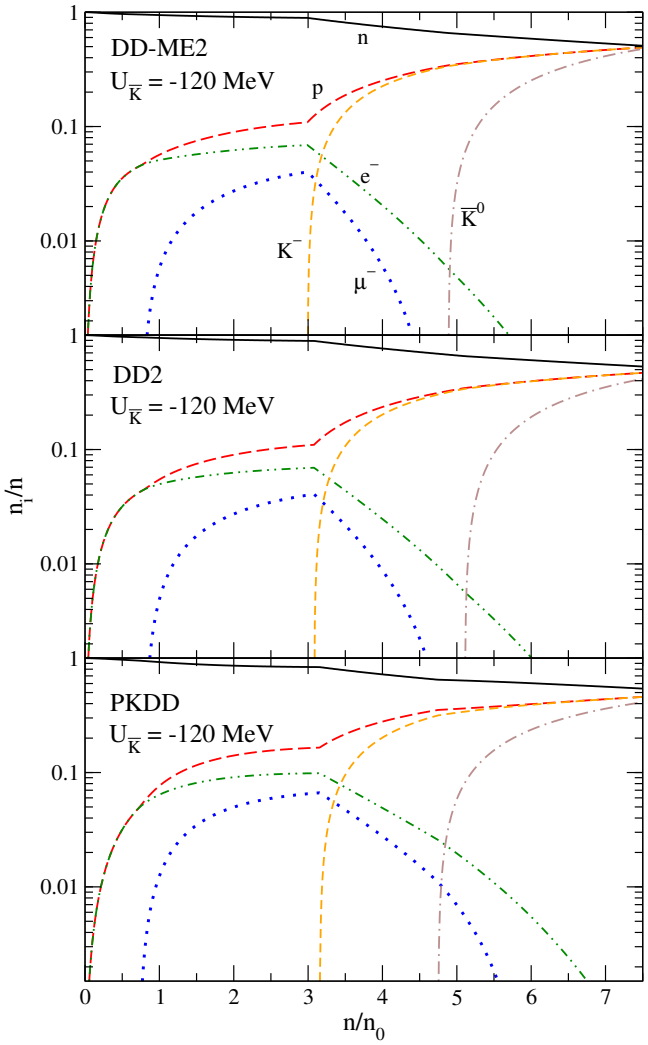

Figure 3.12: Same as fig.3.3. Upper panel: DD-ME2, center panel: DD2, lower panel: PKDD parametrization model and K^- potential depth of -120 MeV. The different curve representations are similar as in fig.-3.3.

gives a realistic M-R relation for all the considered values of $U_{\bar{K}}$.

In most of the cases, the transition to a condensed phase is through second order phase transition. First order phase transition occurs only with $U_K = -160$ MeV for the non-linear model with GMT parametrization. In this case the star possesses a mixed phase region containing both hadronic and condensed phase simultaneously. To explain the mixed phase regime, Gibbs conditions alongside global baryon number conservation and charge neutrality are exploited. The mixed phase region ranges for a length of ~ 1.21 km of stellar radius from 6.13 to 7.34 km in a 2 $M_\odot$ NS. The outer core region upto 7.34 km is the pure hadronic phase while the region in the inner core from 6.13 km to center of the star is the (anti)kaon condensed phase. Moreover, the $\bar{K}^0$ condensation is a second-order phase transition. The compact star with the mixed phase regime satisfies the bounds set on mass-radius by the various recent astrophysical observations. The EoS (with mixed phase) evaluated with GMT model incorporating the $\bar{K}$ condensation which satisfies 2 $M_\odot$ criteria can be employed to study

the glitch phenomena in pulsars.

In case of density-dependent parametrization models (DD-ME2, DD2, PKDD), the (anti)kaon condensation is through second-order phase transition. Among these parametrizations, DD-ME2 produces the stiffest equation of state for both the cases with only nucleons as well as nucleons and (anti)kaons. All parameter sets explain the 2 $M_\odot$ neutron star without the inclusion of (anti)kaons. In case of DD2 model, the configuration with $U_{\bar{K}} = -160$ MeV doesn't satisfy the ~ 2 $M_\odot$ maximum mass star. For the PKDD model producing the softest EoS among the considered coupling models, the astrophysical maximum mass constraint is not satisfied with $U_{\bar{K}} \geq -140$ MeV. Within the framework model considered in this work, the upper limit for $U_{\bar{K}}$ in case of DD-ME2 model is -160 MeV.